NANO · MICRO small
www.small-journal.com

Check for updates

Tip-Induced Nanopatterning of Ultrathin Polymer Brushes

Roland Gröger, Tobias Heiler, Thomas Schimmel, and Stefan Walheim**

Patterned, ultra-thin surface layers can serve as templates for positioning nanoparticlesor targeted self-assembly of molecular structures, for example, block-copolymers. This work investigates the high-resolution, atomic force microscopebased patterning of 2 nm thick vinyl-terminated polystyrene brush layers and evaluates the line broadening due to tip degradation. This work compares the patterning properties with those of a silane-based fluorinated self-assembled monolayer (SAM), using molecular heteropatterns generated by modified polymer blend lithography (brush/SAM-PBL). Stable line widths of 20 nm (FWHM) over lengths of over 20000 μm indicate greatly reduced tip wear, compared to expectations on uncoated SiO_x surfaces. The polymer brush acts as a molecularly thin lubricating layer, thus enabling a 5000 fold increase in tip lifetime, and the brush is bonded weakly enough that it can be removed with surgical accuracy. On traditionally used SAMs, either the tip wear is very high or the molecules are not completely removed. Polymer Phase Amplified Brush Editing is presented, which uses directed self-assembly to amplify the aspect ratio of the molecular structures by a factor of 4. The structures thus amplified allow transfer into silicon/metal heterostructures, fabricating 30 nm deep, all-silicon diffraction gratings that could withstand focused high-power 405 nm laser irradiation.

1. Introduction

Atomic force microscopy (AFM) is a reliable method for imaging surfaces at the atomic level, and a versatile mechanical tool for nanostructure formation, due to the proximity of the tip to the sample surface. AFM-based techniques include nanostructuring, nanopatterning for 2D- and 3D-structures and molecular editing methods like nanoshaving and nanografting of surface layers to create lateral chemical contrasts.[1–3] In most cases, pattern writing is a single step sequential process that delivers immediate results. AFM also provides in situ imaging of the structuring result and parameters as normal force, speed, temperature or electric potential of the tip are adjustable line by line during the structuring process. There is rarely any need for additional chemical procedures, as with electron beam lithography for example. Patterns can be arbitrarily designed and are reproduced on the surface coatings with high resolution and feature sizes in the low nanometer range by the tip of the AFM.

The modified coatings control the interaction of materials with their environment, without altering the bulk properties. They can change surface properties such as wettability, friction, or adhesion, which are of great importance from biomimetic anti-fouling paint for surfaces exposed to the elements,[4] all the way coatings for improved acceptance of implants by the human body.[5] Other examples include templates for structure formation in deposited materials[6] and layers that can reversibly switch their chemical functionality by mechanical forces from an AFM tip.[7]

We were looking for an easy and robust AFM-based process to create nano-scale patterns of chemical contrast on silicon surfaces, for example, for directed or guided self-organization of the phase morphology of block copolymer films.[8–10] The method should be routinely applicable and deliver reliable high-throughput results, without having to follow complicated procedures.

Suitable coatings for such structuring are usually made by spraying, spin coating or dip coating with polymer solutions on flat substrates. Ultra-thin self-assembled monolayers (SAMs) with typical thicknesses of two nanometers are created by chemisorption of thiol molecules on coinage metal surfaces, or silane molecules on oxide surfaces like glass, mica or silicon wafers. Thiol and silane SAMs are well suited for AFM patterning, because they can be homogeneously prepared

R. Gröger, T. Heiler, T. Schimmel, S. Walheim
Institute of Applied Physics (APH)
Karlsruhe Institute of Technology
Wolfgang-Gaede-Str. 1, D-76131 Karlsruhe, Germany
E-mail: thomas.schimmel@kit.edu; stefan.walheim@kit.edu

R. Gröger, T. Schimmel, S. Walheim
Center for Single-Atom Technologies (C.SAT)
Karlsruhe Institute of Technology
Strasse am Forum 7, D-76131 Karlsruhe, Germany

T. Schimmel, S. Walheim
Institute of Nanotechnology (INT) and Karlsruhe Nano Micro Facility (KNMFi)
Karlsruhe Institute of Technology
Herrmann-von-Helmholtz-Platz 1, D-76344 Eggenstein-Leopoldshafen, Germany

T. Schimmel
Materials Research Center for Energy Systems (MZE)
Karlsruhe Institute of Technology
Strasse am Forum 7, D-76131 Karlsruhe, Germany

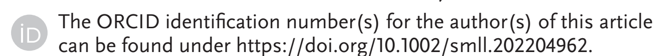
The ORCID identification number(s) for the author(s) of this article can be found under https://doi.org/10.1002/smll.202204962.

© 2023 The Authors. Small published by Wiley-VCH GmbH. This is an open access article under the terms of the Creative Commons Attribution License, which permits use, distribution and reproduction in any medium, provided the original work is properly cited.

DOI: 10.1002/smll.202204962

over wide areas. Thiol SAMs form on sputtered or evaporated polycrystalline gold films with typical roughnesses in the low nanometer range.[11,12] However, the relatively soft gold substrate and its tendency to form grains, makes AFM nanoshaving and the characterization of the resulting pattern difficult. Therefore, we consider thiols SAMs only the second-best choice for nanoshaving. On the other hand, functionalization of oxidized silicon wafer surfaces with silanes can be difficult, often requiring the use of hazardous chemicals. One needs to follow complicated procedures meticulously to achieve sufficiently stable and homogeneous layers, for example in the preparation of octadecyl-trichlorosilane (OTS)-SAMs on native silicon oxide surfaces.[13] The advantage of this substrate is that it is much smoother than the gold surfaces allowing for a much more accurate imaging of the monolayers. Nevertheless, only very little work on the mechanical structuring (nanoshaving) of silane SAMs has been done to date.[14] The reason is the higher bond strength between the molecules and the substrate compared to the thiol molecules on gold. Therefore, in[14] predetermined break points in the molecules are exploited and they are not removed entirely. Additionally, only small areas of 200 nm × 200 nm were patterned. Mechanical large-area structuring can most probably only be achieved with a more weakly bonded layer system.

Polymers can also form ultrathin functional layers by depositing short polymer chains with functional end groups on surfaces, where they form so-called polymer brushes.[15–18] They usually tether to the surfaces by physisorption or covalent chemical bonding of the end groups. Whereas the alkane chains of SAM-forming molecules arrange themselves into ordered layers of defined thickness by interaction with each other, polymer brushes consist of an amorphous layer of polymer chains, where chain length and coverage density determine the layer thickness. With increasing coverage density the steric repulsion between the chains causes them to extend away from the surface.[19] Brushes usually have thicknesses of a few nanometers down to even below 1 nm. They are known to reduce frictional forces on thus coated surfaces,[20] which is important for AFM structuring, since the associated tip wear influences the stability and reproducibility of the structuring process.

As described above, AFM nanoshaving to pattern organic layers has already been applied to thiol SAMs,[1,21–23] for example as nucleation sites for metal deposition,[24] as well as polymer brushes with much higher thicknesses.[25–28]

In recent years, the technologies of dip-pen nanolithography and writing with a hot tip (t-SPL, thermal scanning probe lithography) were promoted.[29,30] The limitation of dip-pen nanolithography lies in it being an additive manufacturing process, since the required periodic dipping of the tip into the ink reservoir makes writing larger areas difficult. Also the resolution is more likely to be in the range above 100 nm, up to 1 µm.[31] Especially in high-resolution work, gold substrates and thiol based inks are often used, with the usual disadvantage of the gold surfaces roughness.

In t-SPL-lithography, some advantages of direct writing are lost due to the need to apply a resist, which is then only incompletely evaporated. Further process steps like plasma treatment are necessary to finally expose the substrate completely. To achieve ultimate resolutions in the 30 nm range, multiple layers of resist and complex process steps are necessary.

1.1. Brush Editing Approach

Here we describe the classic approach of one-step subtractive writing into an ultrathin film on a smooth surface. The substrate preparation is quite easy and the result can be seen immediately after writing. We analyze the effects of tip wear on the width of lines written in an ultrathin brush layer on a silicon substrate during AFM nanoshaving, depending on the normal force applied to the tip and the total line length written. We also apply the process to a polymer brush layer and silane SAM combination, prepared side by side on one sample, which allows for direct comparison of molecular editing results on silane SAMs and PS-brushes.

2. Results and Discussion

2.1. Tip Wear and Molecular Editing Success as a Function of Contact Force

We designed different patterns with emphasis on extended line lengths and wrote them into layers of vinyl-terminated polystyrene-(PS)-brush molecules, grafted on the native oxide layer of a polished silicon (100) wafer surface. The line length of the pattern depicted in **Figure 1**a,b was about 5 mm and was written several times side by side with the same tip, with a normal force of 1 µN and a tip velocity of 4 µm s^{-1}, amounting to a total line length of about 20 mm. The depth of the lines corresponded to the PS brush thickness of 2 to 3 nm, with the substrate visibly undamaged. The linewidth was ≈20 nm (FWHM) and no broadening was observed within the accuracy of the measurement over the total length of all structures written, thus creating a pseudo aspect ratio of $1:10^6$ (width/length of the line). The constant linewidth indicates negligible tip wear, although if the structuring would have been done on an uncoated silicon oxide surface with this tip load much higher wear would be expected.[32]

With increasing normal forces, tip wear becomes detectable, as shown in **Figure 2**. Here a pattern with a line length of 1 mm was written at 4.5 µm s^{-1} tip velocity and a tip load of 1.7 µN. The initial linewidth is 39 nm and broadens to 51 nm toward the end. The relatively high tip load causes initial wear, resulting in a certain linewidth at the beginning of each pattern. Friction between surface and tip during writing leads to abrasion of silicon from the tip, until a steady state is reached, where the contact area is large enough that further abrasion is greatly reduced. Assuming that the linewidth in the pattern in Figure 2 corresponds to the plateau width of the worn tip, together with the geometric dimensions from the tip datasheet, we derived the tip wear rate according to Archard's model[33] to be $\approx 2 \times 10^4$ nm^3 m^{-1} nN^{-1}. This is by a factor of about 5×10^3 less than the expected tip wear rate for friction on an uncoated silicon surface.[34]

We designed a grid-like pattern, consisting of horizontal and vertical lines, requiring equal amounts of tip movement

© 2023 The Authors. Small published by Wiley-VCH GmbH

16136829, 0, Downloaded from https://onlinelibrary.wiley.com/doi/10.1002/smll.202204962 by Karlsruher Inst F. Technologie, Wiley Online Library on [02/05/2023]. See the Terms and Conditions (https://onlinelibrary.wiley.com/terms-and-conditions) on Wiley Online Library for rules of use; OA articles are governed by the applicable Creative Commons License

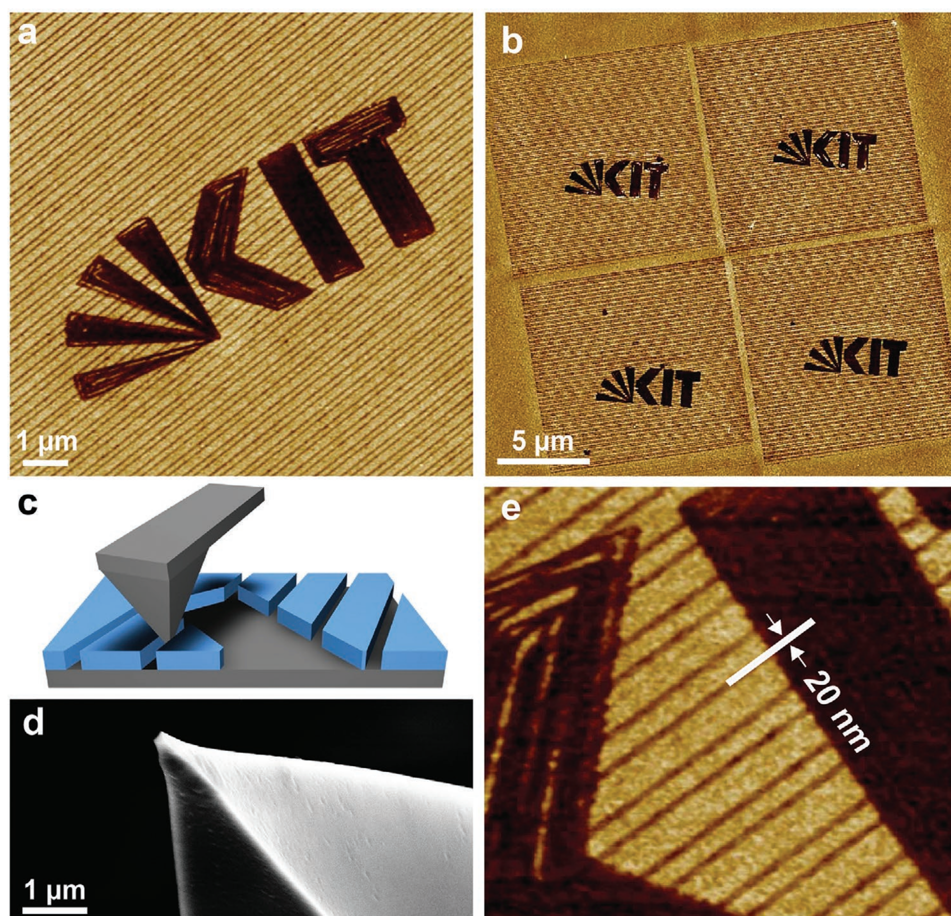

Figure 1. a) AFM topography image of a nanostructured vinyl-terminated PS-brush layer on the native SiO_x surface of a silicon wafer, recorded in intermittent contact mode with a z-range of 3 nm. The brush molecules were removed by applying a normal force of 1 µN to the tip of the AFM, while moving along a predefined line pattern with a tip velocity of 4 µm s^{-1}. The relative high tip load allowed for the reliable removal of the brush molecules in one single run. After structuring several patterns as shown in b) the accumulated contour length reached more than 20 mm. c) Wider areas could be uncovered by writing adjacent lines. d) SEM image of a worn AFM tip. Tip wear typically produced flattened plateaus. e) No broadening of the linewidth of 20 nm (FWHM) was observable within the accuracy of the measurement.

forward, backward, left, and right, to average out directional dependencies of tip wear. The grids patterns were written in brush layers at tip loads increasing from one to 5.5 µN, and the resulting linewidths were measured and plotted versus the normal force in **Figure 3**.

At normal forces between 1 and 5.5 µN the line width increased proportionally from 15 to 98 nm, respectively. Since both the substrate and the tip consist of silicon, we attribute the broadening to tip wear rather than elastic deformation at the contact area. After an initial tip wear depending on the normal force, the contact area size stabilizes, when the contact pressure is not sufficient to remove any more silicon atoms from the tip. In the center of the contact area, the contact pressure is still high enough to remove the brush molecules from the substrate. Toward the edges, we assume the pressure to drop far enough for the molecular bonds to stay intact, due to squeezing the polymer chains out from under the tip. This area supports part of the tip load and helps inhibiting further wear by reducing friction. The tip shape then remains stable during the writing of extended line lengths of over 20 mm. We calculated the contact pressures p in Figure 3 from the tip load F and the square root of the line width d: $p = 4F/\pi d^2$, assuming a circular contact area. The pressure decreases with higher tip loads, due to the square increase of the contact area, where the threshold to break the bonds between the brush molecules and the surface is exceeded. These are upper estimates for the contact pressure, since the width of the load-supporting border around the inner contact area is not exactly known. We estimate it to be at most the contour length of the brush molecule of 5.4 nm. This mechanism can be used to select the desired linewidth via the normal force, albeit the selection can go only one way from narrower to wider lines.

For structuring arbitrary 2D-patterns, it is desirable to write not only lines, but also remove the brush layer from contiguous areas. We achieved this by writing adjacent lines with distances smaller than the width of the active structuring area of the tip. AFM analysis of such areas shows a very high phase contrast, where even a few remaining molecules are detectable in the phase image, as seen in the middle of the structured area in **Figure 4**. The high phase contrast indicates a true removal of the brush molecules from the surface rather than only a displacement to the sides of the structuring tip. The few molecules

© 2023 The Authors. Small published by Wiley-VCH GmbH

16136829, 0, Downloaded from https://onlinelibrary.wiley.com/doi/10.1002/smll.202204962 by Karlsruher Inst F. Technologie, Wiley Online Library on [02/05/2023]. See the Terms and Conditions (https://onlinelibrary.wiley.com/terms-and-conditions) on Wiley Online Library for rules of use; OA articles are governed by the applicable Creative Commons License

16136829, 0, Downloaded from https://onlinelibrary.wiley.com/doi/10.1002/smll.202204962 by Karlsruher Inst F. Technologie, Wiley Online Library on [02/05/2023]. See the Terms and Conditions (https://onlinelibrary.wiley.com/terms-and-conditions) on Wiley Online Library for rules of use; OA articles are governed by the applicable Creative Commons License

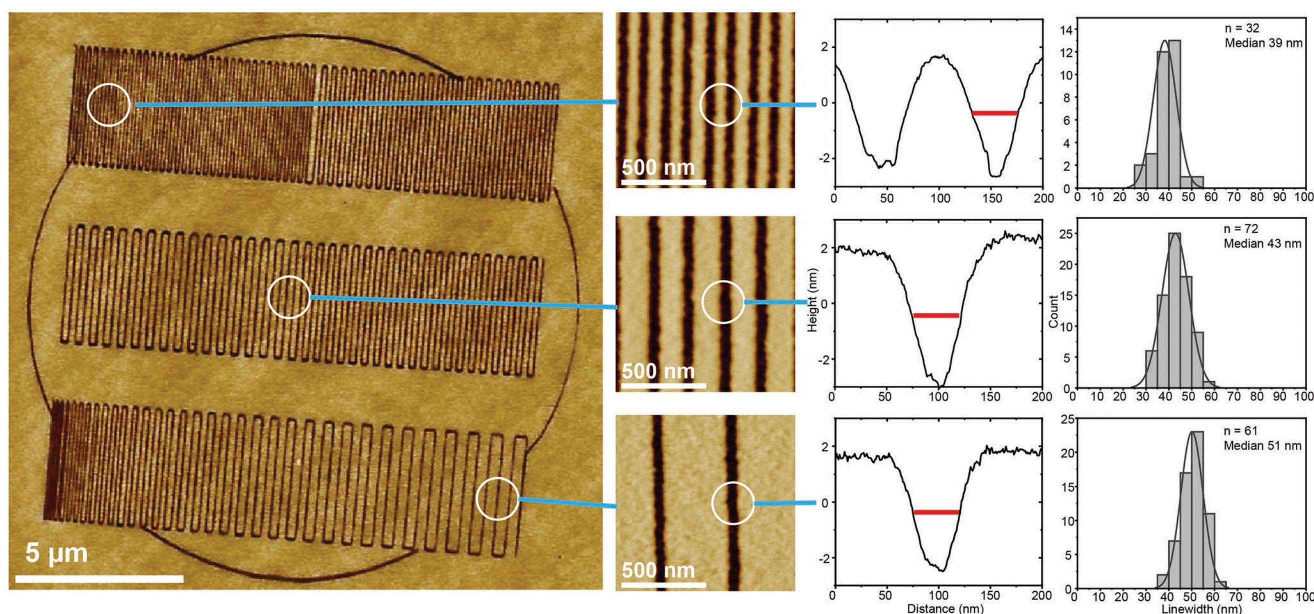

Figure 2. The pattern on the left was written in a PS-brush layer with a normal force of 1.7 µN and a tip velocity of 4.5 µm s^{-1}, starting at the top left to the bottom right. The total line length is 1 mm. Line profiles from the beginning, the mid-section and the end were taken and the widths (FWHM) measured several times and plotted in the histograms at the right. The initial linewidth was 39 nm (median of 32 profiles measured), broadened to 43 nm in the middle (72 profiles measured), and finally came to 51 nm toward the end of the pattern (61 profiles measured). On an unprotected silicon surface, we would expect such tip wear after a much shorter distance, in the range of 200 nm. The lubricating effect of the polymer brush makes it possible to write such long and narrow lines. The interplay between the low bonding strength of the molecules to the substrate and their lubricating effect enables this excellent mechanical structurability.

left attached in the middle reach a height of only 0.3 nm and are likely to be lying flat on the surface in the so-called "pancake" state. It shows the strong chemical contrast even a few brush molecules produce, as desired for directed self-assembly of block-copolymer layer phase separations.

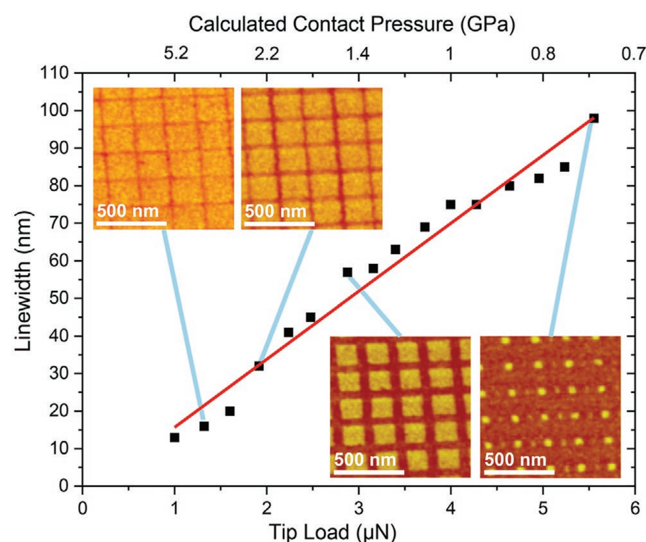

Figure 3. Grid patterns written into brushes with increasing tip loads, resulting in broadening lines. In the range between 1 and 5.5 µN the relation between tip load and line width is linear, rising from 13 to 98 nm respectively. We calculated the contact pressure from the tip load over the contact area, which we assumed to be circular with diameters equal to the linewidths at the respective tip loads.

2.2. Direct Comparison Brush versus SAM Regarding Structuring Properties and Mechanism

In order to further evaluate the nanoshaving properties of the PS-brush, we compared it directly with an FDTS-SAM. Therefore, we prepared a pattern of brush islands with diameters of about 500 nm in a matrix of an FDTS-SAM using a technique called polymer blend lithography (PBL, see Experimental Section). On that substrate, we wrote patterns of parallel lines with sizes of 4 × 4 μm^2 and increasing tip loads, so that the lines spanned alternating brush and FDTS SAM areas. Since both layers are patterned simultaneously, we can compare the nanoshaving results directly, as they were made with the same cantilever at the exact same force load and tip velocity. This eliminates differences that might emanate from variations in tip wear conditions, cantilever spring constants or AFM adjusting variations, in case the sample or the cantilever were to be changed during the experiment. **Figure 5** a and c show AFM topography images of such groups of lines spanning over both the matrix of FDTS-SAM and the round PS-brush areas at normal force loads of 1 µN (a, b) and 3 µN (c,d). We plotted the depths of the structured lines on the PS-brush and the FDTS-SAM versus the applied structuring force in Figure 5e. The respective first data point corresponds to the average layer thickness, determined directly after the brush preparation. The PS-brush was completely removed from the substrate at forces above 1.5 µN, while the 1.2 nm thick FDTS-layer appeared only slightly dented at the surface, even up to maximum applied forces of 5.5 µN. The binding of the FDTS molecules is much more stable, due to the extremely

© 2023 The Authors. Small published by Wiley-VCH GmbH

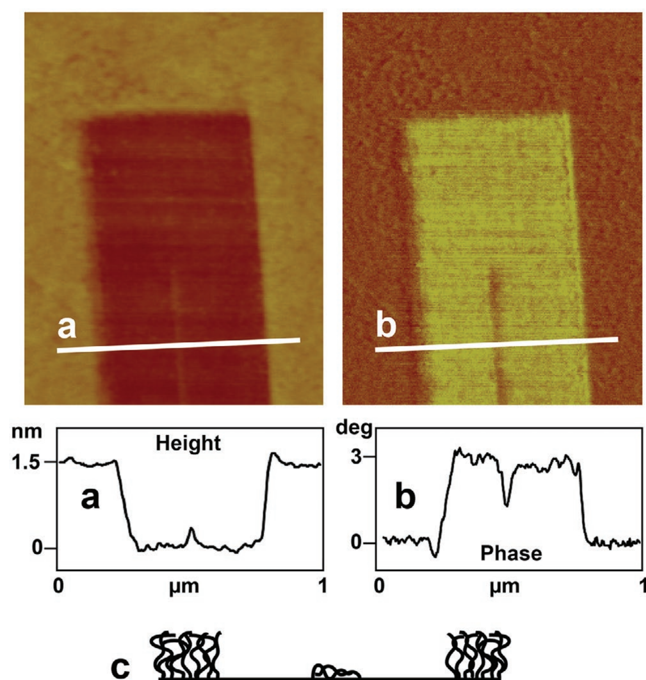

Figure 4. AFM image of a rectangular area, nanoshaved into a PS-brush layer on a native SiO_x wafer surface. The left image shows the AFM topography in tapping mode with a scan size of 1.2×1.5 µm² and a z-range of 5 nm. The right image shows the corresponding phase contrast image. A step height of 1.5 nm between the PS-brush and the SiO_x surface can be measured (profile a). The corresponding bright phase contrast indicates a complete removal of the PS-brush in the rectangular areas (profile b). We left a narrow line of brush standing in the middle of the rectangle. Its height of 0.3 nm is only a fraction of the original brush thickness; however, the phase image shows a much higher contrast, indicating that a few remaining brush molecules provide sufficient surface functionalization, as depicted in scheme (c).

high density of binding sites between SAM and substrate. For good reason silane SAMS are known in silicon-based micromechanics as lubrication and abrasion protection layers. The loosely folded PS brush, on the other hand, has a much lower grafting density, and can therefore be removed more easily and cleanly. The AFM tip probably does not even penetrate the FDTS-SAM completely and its bonds are sheared off only partially.

Part of the force acting on the tip is due to capillary forces of the water meniscus that forms between the tip and the substrate. We measured this force contribution on all three substrates (SiO_x, FDTS and PS-Brush). This measurement resulted in average values of 125 nN on SiO_x, 45 nN on FDTS and 105 nN on the PS-Brush. These are an order of magnitude below the forces used for structuring and were therefore not considered further (see section Statistical Analysis).

At even higher normal forces, increased tip wear started to set in, causing broadening of the lines and double tip artifacts. We observed no effects attributed to the functionalization of the tip with Teflon molecules shaved off the FDTS layer.[35] As additional benefit, this system with its FDTS matrix and AFM-patterned PS brush islands can be used for creating a ternary chemical contrast on the surface.

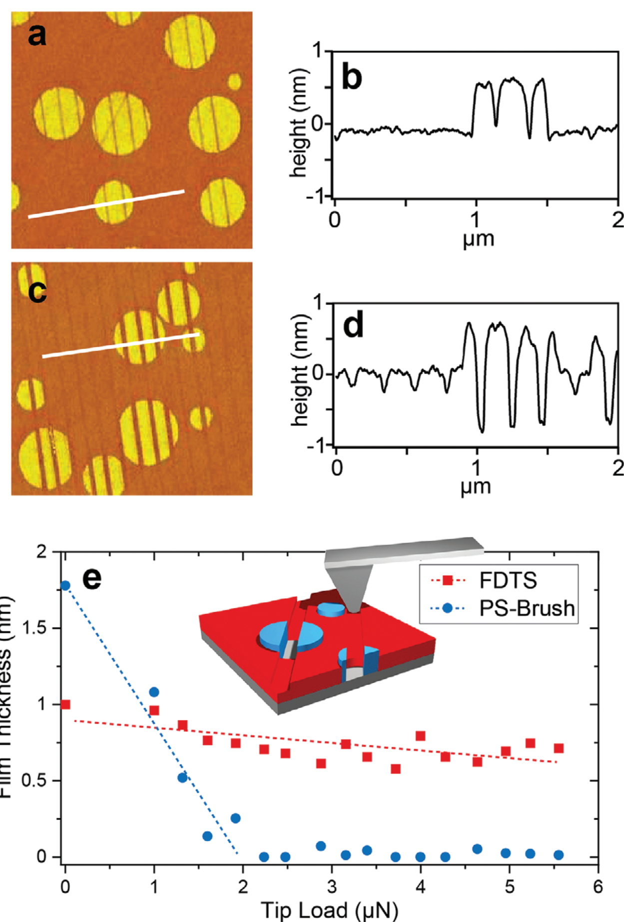

Figure 5. PS-brush islands with diameters of about 500 nm (bright circles in a and c), surrounded by an FDTS SAM matrix were prepared on SiO_x wafer surfaces by a modified PBL[36] process and then structured with the AFM (inset in e). The quality of nanoshaving the PS-brush and the FDTS-SAM was directly comparable (b and d), by writing line patterns over both molecular layers with the same tip load, allowing us to exclude variations due to tip wear or different spring constants. We wrote the line patterns with increasing normal forces of up to 5.5 µN. At forces above 1.5 µN, the PS-brush was completely removed from the SiO_x surface (blue dots in e), while the FDTS-SAM was still stable at maximum loads of 5.5 µN (red dots in e). The silane SAM molecules could not be removed or sheared off, even with the largest normal force available here, since they are bound much stronger, while the polymer brush molecules detach reliably. On an uncoated surface the AFM tip would have worn to at least 200 nm in width after this experiment.[32] The lines are a guide to the eye.

2.3. Directed Self-Assembly of a Polymer Blend System Induced by Brush Editing Pattern (Polymer Phase Amplified Brush Editing, PPABE)

In order to demonstrate the full potential of brush editing, polymer mixtures were deposited on the generated patterns, which should arrange themselves along the patterns. The phase behavior of polymer mixtures in thin films has been studied intensively for some time. In almost all polymer mixtures a demixed morphology is formed during the spincoating process, due to the evaporation of the solvent and the enthalpic interaction, in which both types are finally present in demixed, almost pure form. If a hydrophilic substrate is used, there is a

© 2023 The Authors. Small published by Wiley-VCH GmbH

16136829, 0, Downloaded from https://onlinelibrary.wiley.com/doi/10.1002/smll.202204962 by Karlsruher Inst F. Technologie, Wiley Online Library on [02/05/2023]. See the Terms and Conditions (https://onlinelibrary.wiley.com/terms-and-conditions) on Wiley Online Library for rules of use; OA articles are governed by the applicable Creative Commons License

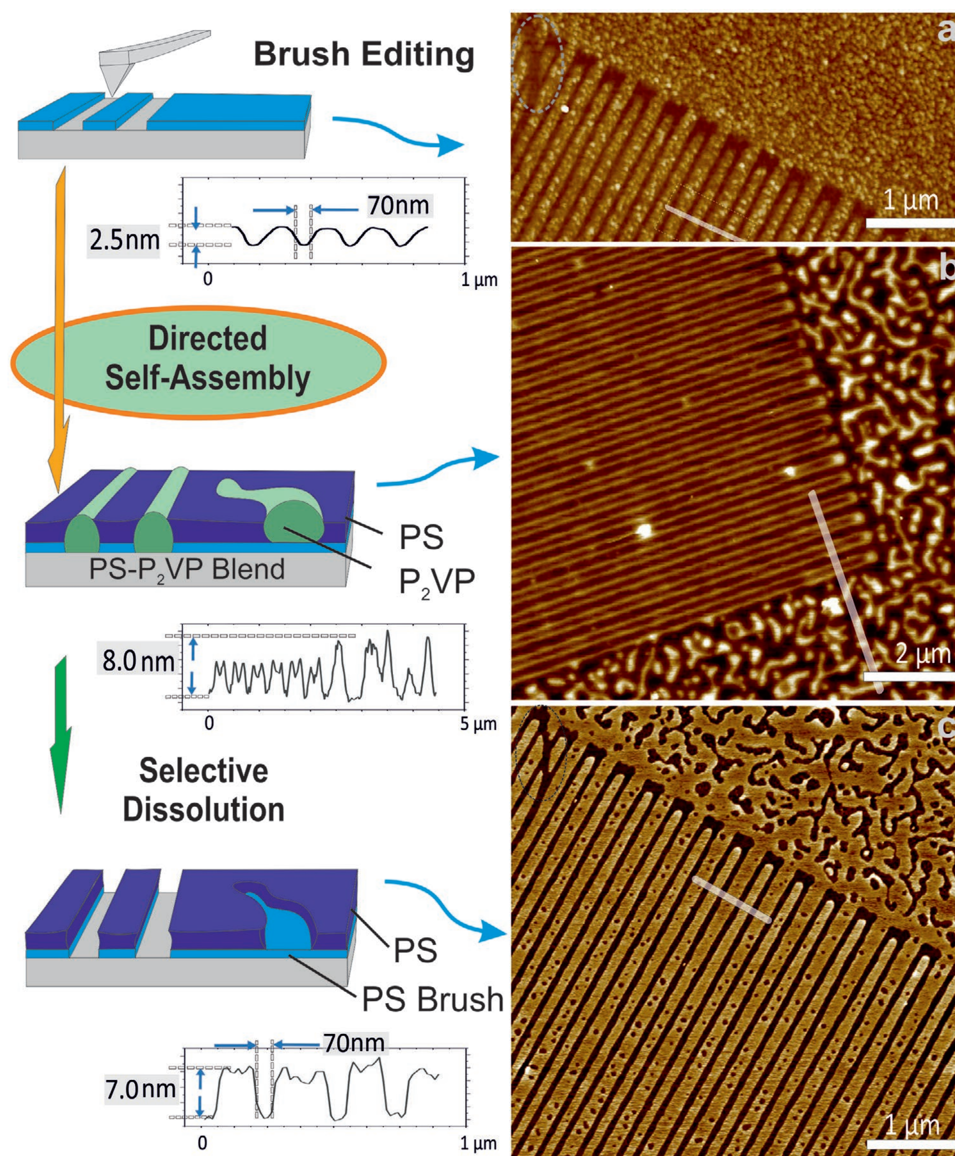

Figure 6. Pattern-induced phase separation (Directed Self-Assembly) of a polymer film consisting of PS and P2VP. The written PS-brush nanopattern on the substrate (a) influences the phase separation of the polymer mixture during a spin coating process (b). This process takes about 1–2 s. The patterned substrate organizes the otherwise random pattern along the previously written lines. The line width of the P2VP lines is about 70 nm. The hydrophilic PVP is attracted to the hydrophilic SiO_x lines exposed by the AFM brush editing process. After selective removal of P2VP with ethanol, the substrate is exposed down to the bottom and a sharp-edged lithography pattern consisting of pure PS with a height of 8 nm is formed (c). The cross-section in (a) was created by averaging in the displayed box. The cross sections in (b) and (c) are single lines. The somewhat rough appearance of the PS brush surface in (a) is due to the fact that the sample in (c) was completely rinsed with THF after the AFM recording in order to make this recording of (a) at the same location. Presumably, residues of intercalated PS molecules remain in the polymer brush and create this roughness.

pronounced tendency for one of the polymer types (the more polar one) to wet the substrate during the spincoating process and for the other (less polar) component to come to rest on the free surface.[37,38]

A patterned surface (hydrophilic/hydrophobic) can control this stratification process in a laterally alternating manner and a lateral morphology that orders itself according to the pre-printed pattern can be forced (directed self-assembly).[39] Here, a highly developed polymer solvent system was used, which can be optimized in its structural fidelity by controlling the air humidity during the spincoating process.[40,41] **Figure6** shows the result of the structure transfer into the polymer blend polystyrene/poly(2-vinylpyridine)/tetrahydrofurane (PS/P2VP/THF). After spin coating the hydrophilic P2VP comes to rest on the hydrophilic areas, where the brush was removed by the AFM, whereas PS comes to rest on the untouched PS brush (b). After selective removal of the P2VP component, the pure PS morphology can be seen in (c), which displays a sharp-edged structure with an increased thickness by a factor of about 4. The 2 nm thick PS brush turns into an 8 nm high PS layer, presumably partially intercalated into the PS brush. The AFM image (a) shows a somewhat higher roughness than expected from

© 2023 The Authors. Small published by Wiley-VCH GmbH

16136829, 0, Downloaded from https://onlinelibrary.wiley.com/doi/10.1002/smll.202204962 by Karlsruher Inst F. Technologie, Wiley Online Library on [02/05/2023]. See the Terms and Conditions (https://onlinelibrary.wiley.com/terms-and-conditions) on Wiley Online Library for rules of use; OA articles are governed by the applicable Creative Commons License

a pristine brush, because it was recorded at the same location as in (**c**), however after the removal of the PS layer with THF. Even this very good solvent for PS cannot completely remove the intercalated PS and a slightly thickened, rougher PS brush structure remains.

The circle in the top left of Figure 6a highlights an incompletely structured curved line which was created unintentionally with low contact force. In Figure 6c that same spot shows, that after spin coating the polymer blend and rinsing off P2VP, even the partial removal of the PS brush attracts the P2VP. The result is a polymer structure with almost digital (black and white) quality. This means that the pattern transfer process is fault-tolerant with regard to incompletely removed brush molecules, which is good news for a later technical application of polymer phase amplified brush editing (PPABE).

Figure 7 shows the application potential of the polymer brush-based lithography presented here. The now amplified polymer structure (a) was used as a lift-off mask for a metal structure in order to finally transfer the pattern about 30 nm deep into the silicon substrate by means of reactive ion etching (RIE). First, 0.5 nm Chromium and 5 nm Gold were deposited onto the amplified structure (e). The polymer structure was then lifted off by CO_2 snow jet to expose the metal pattern in the trenches of the structure. The 5.5 nm thick metal layer remains in the areas where the polymer brush was originally removed and can now be used as a resist for deep etching the silicon substrate. In this process, the reactive gases SF_6 and CHF_3 also successively consume the metal, but 30 nm deep trenches can be created in the silicon, where originally there were about 2 nm deep trenches in the polymer brush. Since the refractive index of silicon is about 3.8, this relatively flat periodic silicon structure is an effective diffraction grating for visible light. In Figure 7j, the color effect of the different lattice constants of the test structure is clearly visible, especially with dark-field illumination and the polarizer in the beam path after reflection. If the polarizer in front of the camera is rotated, the light selected by polarization plane and color from the grating can be almost completely filtered out (k-m) and only scattered light remains.

The test pattern in Figure 7 has areas of different periodicities, showing different colors under the given illumination (dark field, incident light, 20× objective). The bright white field in the lower middle of Figure 7j has a periodicity of 465 nm and is visible most clearly. Here the first diffraction maximum of a broad spectral range hits the objective. To investigate the diffraction efficiency of this grating in more detail, a larger field with a comparable periodicity was written into the brush, amplified with PBABE and deep etched into silicon. A 100 mW laser with 408 nm wavelength was directed at the grating at an angle of 70° to the surface normal. Both the dimension of the grating and the diameter of the laser focus were about 50 µm. A strong reflection spot appears on a screen vertically above the surface, with the p-polarized laser beam in grazing incidence (**Figure8**a). On closer inspection, the second diffraction order is also noticeable, far in the backscattering range at about 52°. When the screen is removed, the laser diffraction by the grating can be clearly seen in the microscope (spot on the flat substrate in Figure 8c, spot on the grating in 8d). The line direction of the grating, as well as the polarization direction of the laser is indicated by the purple double arrow. When defocussing the microscope, the typical color effects due to the angular dispersion of the optical silicon gratings with the periodicities of 470 and 510 nm become visible (Figure 8g).

3. Conclusion

In this work, we investigate the properties of ultrathin polystyrene brush coatings on silicon substrates during AFM nanostructuring, the influence on tip wear and hence linewidth and long-distance stability. We found that after an initial broadening of the tip, which depends on the normal force, the tip is stable over long distances during brush patterning. This initial broadening can be used to define line widths. Below normal forces of 1.5 µN, line widths remained constant over long distances, with written lines 10^6 times longer than their width. However, at normal forces above 1.5 µN, some wear along the line length became measurable. The brush itself provides a molecular lubricating layer that greatly reduces wear by supporting the normal force as the tip moves across the substrate. We measured a reduction in tip wear volume by a factor of 5×10^3 due to the brush, using Archard's model.[33]

The results show that we can pattern ultrathin polymer brushes reliably with the tip of an AFM without damaging the substrate, and with very low tip wear at a factor of 5000 lower than on a SiO_x surface without a PS brush. Our study shows that at the forces applied here with identical tips, a conventional SAM layer can be removed only partially. We were able to produce large patterns with good binary and, in combination with a PBL-pre-patterned substrate, ternary chemical contrasts. This provides us with a robust method to fabricate high-resolution AFM nano-patterned surface structures with high-throughput. Patterns written with our brush editing technique can be used as templates for directed self-assembly.

As a first application example, we demonstrate the creation of a diffraction grating in silicon. The procedure uses the pattern-induced phase separation of a thin polymer blend film during spin coating with a line width of 70 nm. By removing one of the polymer phases, the original 2 nm high structure is amplified to 8 nm, which allows this structure to be used as a lift-off mask for a Cr/Au layer. The metal layer remains exactly where the polymer brush was originally removed and can then be used as a resist for deep etching into the silicon substrate. Line patterns with 470 nm periodicity could be successfully etched 30 nm deep into silicon. These show polarization effects, effective diffraction of white light and an intense laser beam (100 mW at 405 nm with a 50 µm spot).

As it is possible to produce much smaller structures with brush editing, this substrate is interesting to address a very similar issue: the forced ordering in thin block copolymer layers. In the past, it was shown that surface-induced phase separation is also possible in this case. Initially with coarse patterns in the micrometer range.[42] Increasingly, however, efforts have been made to achieve smaller and smaller structures with pre-structuring,[43,44] Highly sophisticated lithography processes such as EUV lithography were and are still being used,[45] which of course severely limits their practical applicability. With brush editing, a new, easily achievable structuring can now be used to induce order in the phase behavior of thin block copolymer

© 2023 The Authors. Small published by Wiley-VCH GmbH
16136829, 0, Downloaded from https://onlinelibrary.wiley.com/doi/10.1002/smll.202204962 by Karlsruher Inst F. Technologie, Wiley Online Library on [02/05/2023]. See the Terms and Conditions (https://onlinelibrary.wiley.com/terms-and-conditions) on Wiley Online Library for rules of use; OA articles are governed by the applicable Creative Commons License

16136829, 0, Downloaded from https://onlinelibrary.wiley.com/doi/10.1002/smll.202204962 by Karlsruher Inst F. Technologie, Wiley Online Library on [02/05/2023]. See the Terms and Conditions (https://onlinelibrary.wiley.com/terms-and-conditions) on Wiley Online Library for rules of use; OA articles are governed by the applicable Creative Commons License

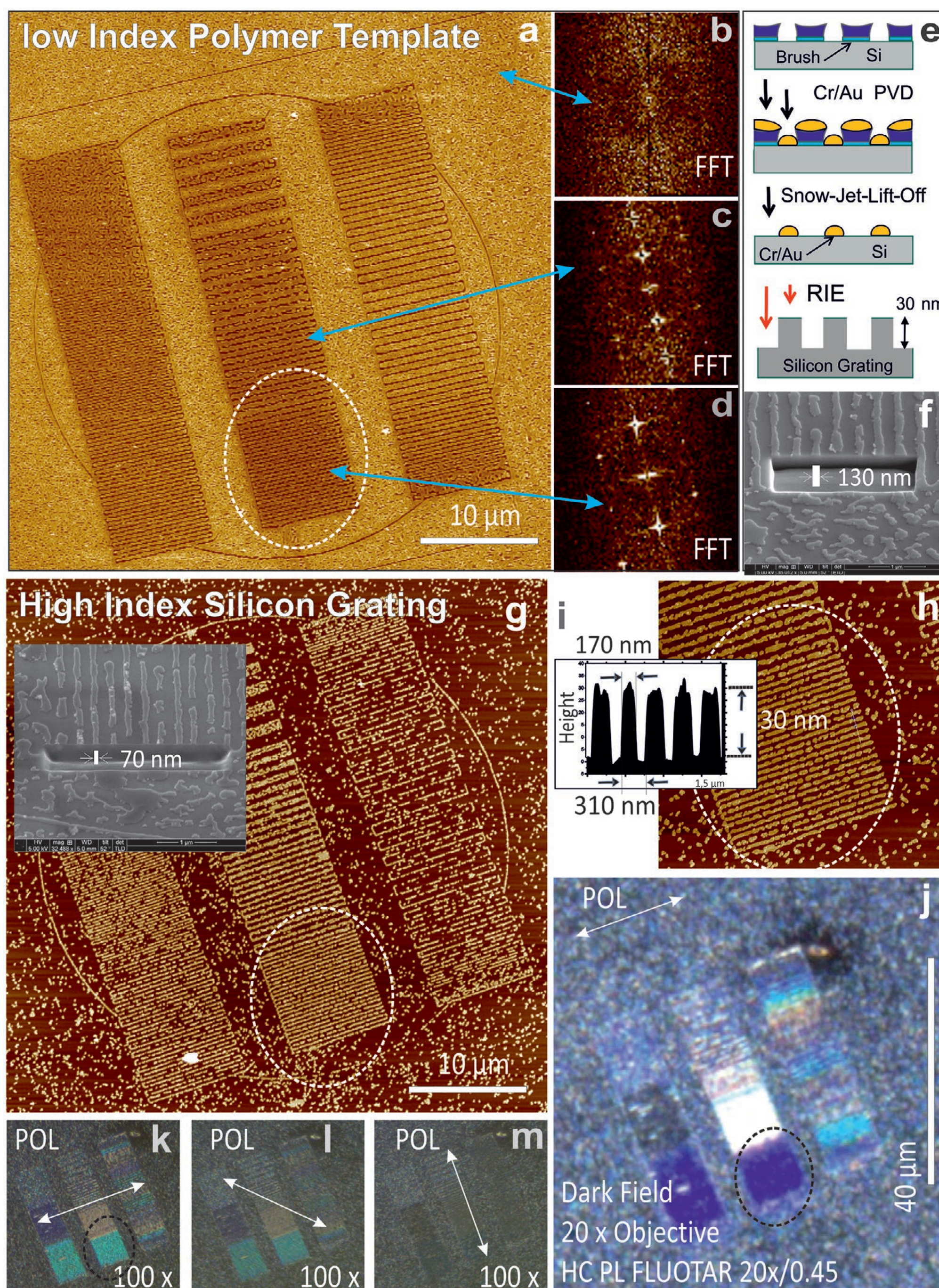

Figure 7. From Polymer Blend Amplification (8 nm) to Silicon Grating (30 nm): Depicted is a larger section of a sample as shown in Figure 6c with the polymer phase pattern of PS already developed by selective dissolution of P2VP. The periodic line patterns show a clear signature in the Fourier transformed (FFT) image from sections with line periodicities of 310 nm and 465 nm respectively (bright spots in (c) and (d)). In contrast to the FFT image in (b), which stems from the disordered region in the upper right of (a), where there is only a diffuse circle associated with a mean polymer phase domain correlation length of about 300 nm. After the sample was AFM characterized, it was coated with 0.5 nm Chromium and 5 nm Gold and the polymer pattern removed with the CO_2 snow jet. The remaining metal structure could then be used as an etch resist for RIE to etch the structure into the silicon substrate (e). By incising with a focused Pt-ion beam, scanning electron microscope sections of the resulting structure could be obtained (f, g). The topographic AFM image shows an etch depth of 30 nm and a periodicity of 310 nm (170 nm line width) (h,i). The inset in (g) shows a high density structure area with 70 nm linewidth taken in the area underneath the inset. In the optical microscope, dark field illumination shows a strong color effect, due to the angular dispersion of the gratings. With a 20× objective, for example, the grating with 310 nm period appears blue (circle in j). Viewed through a 100× objective, the same structure appears greenish (k) due to the increased angular acceptance of the objective. By rotating the polarization filter perpendicular to the line orientation of the grating, the coloured light, being polarized along the lines, disappears from (k) over (l) to (m).

© 2023 The Authors. Small published by Wiley-VCH GmbH

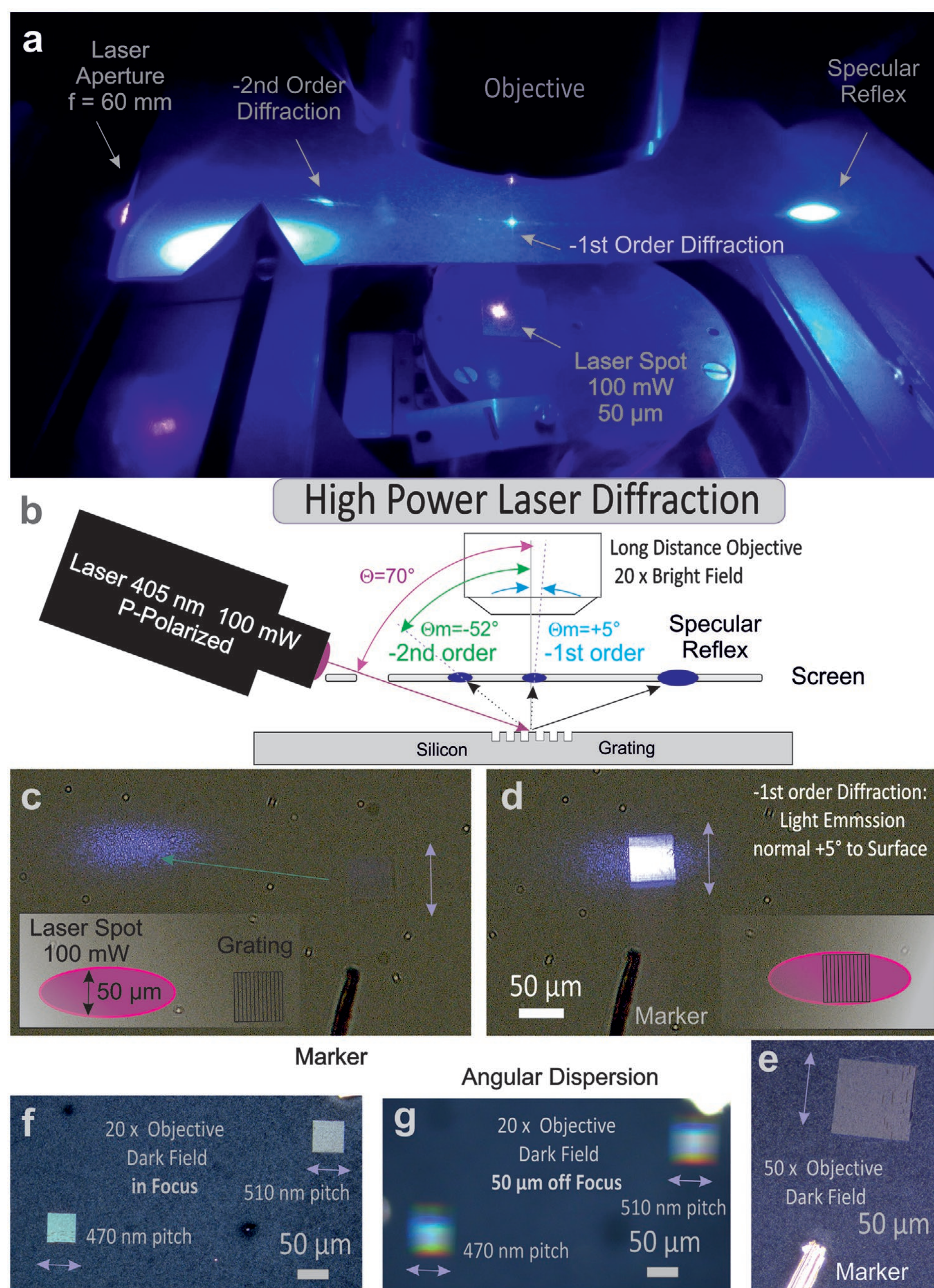

Figure 8. a,b) High power laser diffraction experiment on nanofabricated silicon grating. The 30 nm high silicon nano-grid was derived from polymer brush patterns with a total height of only 2 nm. The diffraction of an intense, focused laser beam (100 mW / 50 µm) that would have simply vaporized the original organic grating is shown in (a). Since the grating constant with 470 nm (235 nm lines) is close to the laser wavelength, the light is diffracted back at oblique incidence and the light of the first diffraction order hits the objective almost vertically when the laser spot is moved onto the grating from (c) to (d) (bright field). In f,g) the second order diffraction peak appears at 52° as expected from the usual grating formula (angle of incidence 70°, grating frequency: 2150 lines mm^{-1}). The rainbow colors for both gratings show the angular dispersion effect under white light, when the microscope is defocussed (white light dark field illumination, objective moved up by 50 µm). In (e) a close up of the grating in (d) is shown.

layers. Due to the intrinsic micro-phase separation of this material class with structure sizes of 20 to 40 nm (mostly cylinders, spheres or lamellae), much higher aspect ratios can be expected than with polymer blends. There is also a large variation of functional polymers in this substance class, which makes an ordered structure formation even more attractive.

4. Experimental Section

Brush Preparation: As substrates we used 10 × 10 mm^2 pieces of silicon wafers with [100] surface orientation and native oxide layers with 2 – 3 nm thickness (Wacker Burghausen, Germany). They were cleaned with a CO_2 dry ice jet to remove organic residue.[46] About 100 µL of a solution (c = 0.01 w/w in toluene) of vinyl-terminated

© 2023 The Authors. Small published by Wiley-VCH GmbH

16136829, 0, Downloaded from https://onlinelibrary.wiley.com/doi/10.1002/smll.202204962 by Karlsruher Inst F. Technologie, Wiley Online Library on [02/05/2023]. See the Terms and Conditions (https://onlinelibrary.wiley.com/terms-and-conditions) on Wiley Online Library for rules of use; OA articles are governed by the applicable Creative Commons License

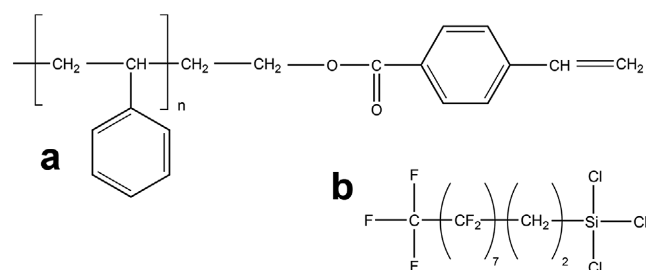

Figure 9. a) Vinyl-terminated polymer brush molecule. The vinyl end-group bonds to the native silicon oxide sample surface. *n* is about 25 for the molecule with $M_w = 2600$ amu. b) SAM-forming silane molecule 1H-1H-2H-2H-perfluorodecyl-trichlorosilane (FDTS).

polystyrene molecules (M_w = 2600 amu; M_n = 2400 amu, Polymer Source, Montreal, Canada) (**Figure 9**a) were cast on the surfaces and left evaporating.

This procedure resulted in a polymer film with a thickness of about two micrometers. The coated silicon samples were then annealed for several hours in a home built aluminium vacuum chamber on a hot plate at 150 °C, evacuated with a scroll pump to a pressure of less than 1 mbar, to allow the brush molecules to bond to the substrate. As described by Maas et al.[47] the functional vinyl end-groups of the polystyrene molecules are transformed into an alcohol, which then reacts with the silanol groups at the SiO_x-surface in a condensation reaction. The preparation time may be reduced significantly in the future, as brush formation was shown to happen on time scales of minutes in a recent publication, using similar, OH-terminated polystyrene molecules.[48]

In order to remove ungrafted, physisorbed molecules the samples were washed using a 3-step counter flow rinsing procedure (cascaded rinsing) in toluene. The samples were dried in a stream of nitrogen after each rinsing process, resulting in brush layers with 1.5–2.5 nm thickness and a surface roughness of 0.1 nm (rms). The brush layers were thermally stable up to at least 160 °C as shown by AFM measurements. The effort for reproducible polymer brush preparation, concerning the control of humidity, temperature and solvent purity was greatly reduced with respect to what is typically necessary for the preparation of SAMs.[49–51]

Polymer Blend Lithography for Brush/SAM patterned Test Surfaces (brush/SA-M-PBL as Molecular Rulers): For direct comparison of SAM- and brush editing, a modified PBL procedure (**Figure10**a) was developed, to prepare polymer brush islands of about 500 nm in diameter, embedded in an FDTS-SAM matrix (molecule in Figure 9b). With this method, surfaces with lateral alternating SAM and brush functionality were created. First, standard PBL was applied to create a structured polymer blend film with a thickness of 70 nm, as in Figure 7a.[36] After selective removal of the PMMA component with acetic acid, the free surface areas between the PS-islands were decorated with a FDTS SAM, using a CVD process. Then the PS islands were selectively removed with the snow jet method, leaving a patterned SAM with a thickness of about 1.2 nm.[36,52] This structure was then coated with a film of brush-forming polystyrene molecules with the same procedure explained above, were molecules graft a brush in the SiO_x-regions of the substrate only. After rinsing with toluene, the structured brush/SAM surface was finished. The brush layer is about 2.5 nm thick and protrudes about 1.3 nm above the FDTS SAM. Here, the brush film was left a little thicker (2.5 nm), by not rinsing as long as usual (1 min), to give a clear topographic contrast between brush and SAM areas (Figure 10b–e).

AFM Structuring (Brush Editing): AFM structuring was done in a single step process in ambient conditions at 21 °C room temperature and 65 % relative humidity, with a home-built AFM-system featuring a closed loop feedback linear xy-piezo stage and a tube scanner for z-positioning and setting the normal force. The system was programmable to write custom designable patterns with nanometer accuracy. Commercially available non-contact cantilevers were used with spring constants of 26 N m^{-1} and resonance frequencies of 300 kHz (OLYMPUS OMCL-AC160TS, now available as OPUS 160AC-NA, µ-masch, Sofia, Bulgaria).

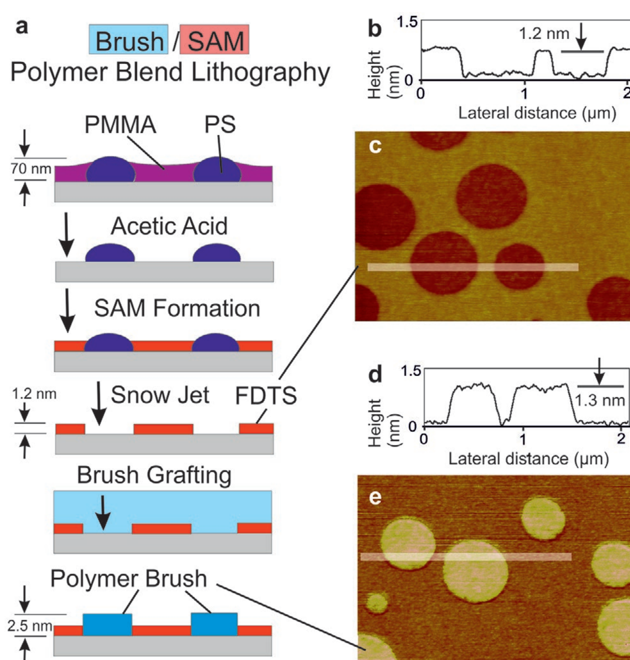

Figure 10. With a new variant of PBL[36]: (brush/SAM-PBL) we created a surface with lateral alternating surface functionality SAM versus brush ((brush/SAM-PBL). At first, a structured polystyrene film was produced (a), where on the free surface between the PS-islands a SAM of FDTS molecules is formed by a CVD process. After removing the PS-islands a structured SAM with a thickness of about 1.2 nm was left. The AFM image in (c) shows the surface of the structured SAM. When coating the structure with a film of brush-forming polystyrene, the molecules graft a polymer brush in the SiO_x-regions of the substrate. After rinsing with toluene the patterned brush/SAM surface was finished. The image in (e) shows the AFM topography, recorded in tapping mode with a scan size of 3 × 2 µm^2. As indicated in the profile in (d) the difference in height between FDTS SAM and PS-Brush was about 1.3 nm, bringing the total brush thickness to about 2.5 nm. The height profiles in (b) and (d) are from the highlighted areas in (c) and (e).

The AFM tip was brought in contact with the surface and applied a defined normal force to the tip while moving laterally according to the predesigned pattern.[3] Since structures in such thin polymer layers were invisible with optical methods, a small mark in form of a short scratch with a diamond glass cutter was placed near the center of the samples. The patterns were written close to one end of the mark, while recording an optical image of the position of the cantilever with respect to the scratch with a video microscope. This allowed retrieving the patterns for the subsequent AFM analysis. The best resolution and reliability at tip velocities of ≈4–4.5 µm s^{-1} were achieved. At higher velocities, the tip began to slide over the brush layer without structuring.

After a cleaning step by washing in toluene and drying in a nitrogen jet to remove any debris of the brush layer from structuring, the samples were analyzed with commercial AFMs (Veeco Multimode IIIa, Santa Barbara, CA and Bruker Dimension ICON, Karlsruhe, Germany). The patterns could be located by placing the tip on the previously recorded position relative to the mark on the substrate. Topography and phase shift images were recorded in tapping mode with new cantilevers of the same type as for structuring.

Brush Edited Pattern Induced Directed Self-Assembly of a Polymer Blend: To demonstrate the applicability of the brush editing patterns, a mixture of poly(2-vinylpyridine) and polystyrene (PSS, Mainz) was spun onto the surfaces.[39,41] The molecular weights were M_w = 10.000 amu for both P2VP and PS. A solution of 0.075 wt% of each polymer in tetrahydrofurane (Sigma Aldrich, p.a.) was spun onto the surface

 © 2023 The Authors. Small published by Wiley-VCH GmbH

16136829, 0, Downloaded from https://onlinelibrary.wiley.com/doi/10.1002/smll.202204962 by Karlsruher Inst F. Technologie, Wiley Online Library on [02/05/2023]. See the Terms and Conditions (https://onlinelibrary.wiley.com/terms-and-conditions) on Wiley Online Library for rules of use; OA articles are governed by the applicable Creative Commons License

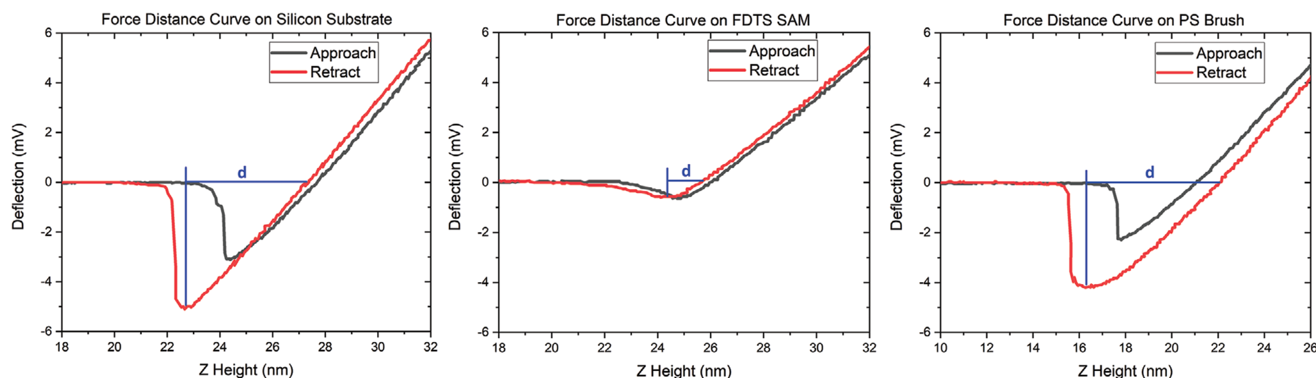

Figure 11. Three exemplary force distance curves on each substrate with the measured distance *d* indicated. The FDTS SAM shows the least interaction with the tip as expected. On the PS brush the adhesion is of the same magnitude as on the bare silicon substrate. The retracting plot on the brush layer is curved, and slightly shifted to the right of the approach plot, indicating elasticity and compression of the brush under the force of the tip.

energy-patterned substrates at 7000 rpm. Polymer segregation was performed in a spin coater with adjustable relative humidity of 29 %rh, and a temperature of 22 °C, measured above the substrate. After placing the sample into the spin coater, nitrogen was introduced into the chamber with 5 L min^{-1} as process gas atmosphere, until a defined dry atmosphere prevailed. A droplet 15 µL of the polymer solution was deposited on the 2×2 cm^2 substrate and the spin process was started.

After the demixing process (lasting ≈1.2 s), P2VP and PS can be dissolved selectively with ethanol and cyclohexane, respectively, without changing the other polymer and showing the desired polymer pattern. With THF, both polymers can be dissolved, however, a certain residue of about 0.5 nm remains on the PS brush (Figure 6a).

Transfer of the Polymer Patterns Into Metal Structures and Silicon Structures: Metal Evaporation: E-beam evaporation of Cr with a rate of 0.02 nm s^{-1} and Gold with a rate of 0.03 nm s^{-1} was performed at a base pressure of 5×10^{-6} mbar. Lift Off was done by snow jet treatment as described above. After lift off the remaining Cr/Au (0,5/5 nm) metal layer was used as resist for RIE etching into the Silicon substrate. RIE: A combination of SF_6 (15 sccm) and CHF_3 (40 sccm) with 130 W forward power was used (Plasma Pro 80, Oxford Instruments). The parameters were: (Si-Etch) P_{RF}: 130 W, DC Bias 0 V 150 mTorr, duration 20 s, strike with 30 mTorr, 5 s, DC Bias 0 V. Prior to Si etching a short descum process was used. Parameters: (Descum): 4/16 sccm O2/N2 P_{RF}: 10 W, 15 mTorr, duration 5 s, strike with 60 mTorr, DC Bias 60 V. For FIB-milling an FEI Strata 400 STEM was used with the parameters: 1.5 pA Ga+ ions, duration 10 min, (SEM imaging: 15 kV, 1.6 nA, ETD SE detector and TLD detector. Optical analysis was performed with a Leica DM6 M microscope with reflected light/dark field and reflected light/bright field illumination with polarization filter. For laser diffraction experiments an MDL-III-405 laser of 100 mW (Thor Labs) with a 60 mm focusing lens was used. And the in situ optical analysis was done using a 20× lens with long working distance from Mitutoyo (infinity corrected BD Plan APO SL 20X/0.28 f = 200).

Statistical Analysis: For measuring profiles of structured lines and polymer layers, the profile functions of Digital Instruments NanoScope III 5.12r3 and Bruker NanoScope Analysis 2.0 were used. With these either single line profiles or averages of several parallel lines can be measured within the AFM height data. To reduce noise, averaged profiles of about 5 to 10 lines were used, as indicated by the wide profile bars in the respective figures.

For the analysis in Figure 2, the line widths (Full Width at Half Maximum, FWHM) were measured with single line profiles several times at different positions along three stretches of lines at the beginning, the middle and the end of the test pattern. The results with sample sizes of $n = 32$, 72, and 61 respectively were plotted in the histograms and the median calculated.

Influence of the Capillary Force: In order to estimate the magnitude of the capillary adhesion force between AFM tip and sample surface, and how it influences the externally applied normal force on the tip, force-distance-measurements were performed on the three surfaces discussed in this work. About 10 force distance curves were recorded with each of three different cantilevers, on the bare silicon substrate, the FDTS-SAM and the PS-brush. Measurements were done in the same ambient conditions as the structuring, at a temperature of 21 °C and a relative humidity of 65% rh. The distances of the snap-off points to the intersection of the retracting curves with the neutral position of the cantilevers were measured as indicated in **Figure 11**.

Capillary adhesion forces were calculated from these distances times the mean force constant of the cantilevers of 26 N m^{-1} (OPUS 160AC-NA, OLYMPUS OMCL-AC160TS). The results were as follows (**Table 1**):

The force constants of the cantilevers themselves are subject to variation. However, in the author's experience the mean value given in the cantilever datasheet was reliable enough to accept this uncertainty as minor. The adhesion forces on the bare silicon substrate and the PS brush lie in the same range between 75 and 169 nN, whereas the adhesion on the FDTS SAM was the lowest as expected, between 26 and 69 nN. The retracting plot on PS brush was slightly curved and shifted, indicating a certain degree of elasticity and compression of the brush layer, which could also be expected. It also shows, that the PS brush molecules do not increase the adhesion of the tip, which was somewhat unexpected.

It is concluded from these measurements, that the capillary adhesion forces are about one magnitude smaller than the normal forces that was applied to the cantilevers during structuring and can thus be disregarded.

Table 1. Capillary adhesion forces on different substrates, calcuated from the data in Fig. 11.

Substrate	Cantilever #	Sample size n	d measured [nm]	Mean adh. Force [nN]
Si + nat. ox.	1	11	4.76 ± 0.18	124
	2	11	3.21 ± 0.27	84
	3	14	6.49 ± 0.13	169
FDTS SAM	4	9	2.66 ± 0.07	69
	5	11	1.01 ± 0.18	26
	6	13	1.37 ± 0.08	36
PS Brush	7	10	3.52 ± 0.13	92
	8	14	2.88 ± 0.16	75
	9	17	5.78 ± 0.13	151

© 2023 The Authors. Small published by Wiley-VCH GmbH

16136829, 0, Downloaded from https://onlinelibrary.wiley.com/doi/10.1002/smll.202204962 by Karlsruher Inst F. Technologie, Wiley Online Library on [02/05/2023]. See the Terms and Conditions (https://onlinelibrary.wiley.com/terms-and-conditions) on Wiley Online Library for rules of use; OA articles are governed by the applicable Creative Commons License

Acknowledgements

The authors acknowledge the support of the Karlsruhe Micro and Nano Facility (KNMFi) Project-ID: 2020-025-029752 and the Werner Siemens Foundation (WSS) within the Center for Single-Atom Technologies (C.SAT). The authors acknowledge Simone Dehm and Min-Ken-Li (INT) for their help with Reactive Ion Etching (RIE) and Torsten Scherer (INT) for his help with Focused Ion Beam (FIB). The logo of the Karlsruhe Institute of Technology (KIT) is used with permission.

Open access funding enabled and organized by Projekt DEAL.

Conflict of Interest

The authors declare no conflict of interest.

Data Availability Statement

The data that support the findings of this study are available from the corresponding author upon reasonable request.

Keywords

atomic force microscopy, directed self-assembly, nanoshaving, polymer blend lithography, polymer brushes, polymer phase amplified brush editing, self-assembled monolayers

Received: August 12, 2022
Revised: February 2, 2023
Published online:

[1] S. Xu, G. Y. Liu, *Langmuir* **1997**, *13*, 127.
[2] D. Pires, J. L. Hedrick, A. De Silva, J. Frommer, B. Gotsmann, H. Wolf, M. Despont, U. Duerig, A. W. Knoll, *Science* **2010**, *328*, 732.
[3] M. Müller, T. Fiedler, R. Gröger, T. Koch, S. Walheim, C. Obermair, T. Schimmel, *Surf. Interface Anal.* **2004**, *36*, 189.
[4] W. Barthlott, M. Mail, C. Neinhuis, *Philos. Trans. R. Soc. London, Ser. A* **2016**, *374*, 41.
[5] Y. Su, I. Cockerill, Y. Zheng, L. Tang, Y. - X. Qin, D. Zhu, *Bioact. Mater.* **2019**, *4*, 196.
[6] N. J. Blumenstein, C. G. Hofmeister, P. Lindemann, C. Huang, J. Baier, A. Leineweber, S. Walheim, C. Wöll, T. Schimmel, J. Bill, *Beilstein J. Nanotechnol.* **2016**, *7*, 102.
[7] J. Berson, M. Moosmann, S. Walheim, T. Schimmel, *Nano Lett.* **2019**, *19*, 816.
[8] M. P. Stoykovich, M. Müller, S. O. Kim, H. H. Solak, E. W. Edwards, J. J. de Pablo, P. F. Nealey, *Science* **2005**, *308*, 1442.
[9] S. Gottlieb, M. Lorenzoni, L. Evangelio, M. Fernandez-Regulez, Y. K. Ryu, C. Rawlings, M. Spieser, A. W. Knoll, F. Perez-Murano, *Nanotechnology* **2017**, *28*, 175301.
[10] G. S. Doerk, C. C. Liu, J. Y. Cheng, C. T. Rettner, J. W. Pitera, L. E. Krupp, T. Topuria, N. Arellano, D. P. Sanders, *ACS Nano* **2013**, *7*, 276.
[11] J. Q. Chen, Q. S. Huang, R. Z. Qi, Y. F. Feng, J. T. Feng, Z. Zhang, W. B. Li, Z. S. Wang, *Nucl. Sci. Tech.* **2019**, *30*, 6.
[12] T. Tian, B. Singhana, L. E. Englade-Franklin, X. Zhai, T. R. Lee, J. C. Garno, *Beilstein J. Nanotechnol.* **2014**, *5*, 26.
[13] S. Pillai, R. K. Pai, *Ultramicroscopy* **2009**, *109*, 161.
[14] L. G. Rosa, J. Y. Jiang, O. V. Lima, J. Xiao, E. Utreras, P. A. Dowben, L. Tan, *Mater. Lett.* **2009**, *63*, 961.
[15] F. Schreiber, *Prog. Surf. Sci.* **2000**, *65*, 151.
[16] E. P. K. Currie, W. Norde, M. A. C. Stuart, *Adv. Colloid Interface Sci.* **2003**, *100*, 205.
[17] W. L. Chen, R. Cordero, H. Tran, C. K. Ober, *Macromolecules* **2017**, *50*, 4089.
[18] O. Azzaroni, *J. Polym. Sci.. Part A: Polym. Chem.* **2012**, *50*, 3225.
[19] M. Himmelhaus, T. Bastuck, S. Tokumitsu, M. Grunze, L. Livadaru, H. J. Kreuzer, *Europhys. Lett.* **2003**, *64*, 378.
[20] J. Klein, E. Kumacheva, D. Mahalu, D. Perahia, L. J. Fetters, *Nature* **1994**, *370*, 634.
[21] S. Krämer, R. R. Fuierer, C. B. Gorman, *Chem. Rev.* **2003**, *103*, 4367.
[22] S. Diegoli, C. A. E. Hamlett, S. J. Leigh, P. M. Mendes, J. A. Preece, *Proc. Inst. Mech. Eng. Part G: J. Aerosp. Eng.* **2007**, *221*, 589.
[23] L. G. Rosa, J. Liang, *J. Phys.: Condens. Mater.* **2009**, 21.
[24] C. Shen, M. Buck, *Beilstein J. Nanotechnol.* **2014**, *5*, 258.
[25] M. Hirtz, M. K. Brinks, S. Miele, A. Studer, H. Fuchs, L. Chi, *Small* **2009**, *5*, 919.
[26] X. F. Sui, S. Zapotoczny, E. M. Benetti, P. Schon, G. J. Vancso, *J. Mater. Chem.* **2010**, *20*, 4981.
[27] T. Chen, I. Amin, R. Jordan, *Chem. Soc. Rev.* **2012**, *41*, 3280.
[28] Q. Yu, L. K. Ista, R. P. Gu, S. Zauscher, G. P. Lopez, *Nanoscale* **2016**, *8*, 680.
[29] C. Rawlings, U. Duerig, J. Hedrick, D. Coady, A. W. Knoll, *IEEE Trans. Nanotechnol.* **2014**, *13*, 1204.
[30] S. T. Howell, A. Grushina, F. Holzner, J. Brugger, *Microsyst. Nanoeng.* **2020**, *6*, 21.
[31] G. Q. Liu, M. Hirtz, H. Fuchs, Z. J. Zheng, *Small* **2019**, *15*, e1900564.
[32] J. P. Killgore, R. H. Geiss, D. C. Hurley, *Small* **2011**, *7*, 1018.
[33] J. F. Archard, *J. Appl. Phys.* **1953**, *24*, 981.
[34] H. Bhaskaran, B. Gotsmann, A. Sebastian, U. Drechsler, M. A. Lantz, M. Despont, P. Jaroenapibal, R. W. Carpick, Y. Chen, K. Sridharan, *Nat. Nanotechnol.* **2010**, *5*, 181.
[35] A. Bubendorf, S. Walheim, T. Schimmel, E. Meyer, *Beilstein J. Nanotechnol.* **2018**, *9*, 1.
[36] C. Huang, M. Moosmann, J. Jin, T. Heiler, S. Walheim, T. Schimmel, *Beilstein J. Nanotechnol.* **2012**, *3*, 620.
[37] K. Tanaka, A. Takahara, T. Kajiyama, *Macromolecules* **1996**, *29*, 3232.
[38] S. Walheim, M. Böltau, J. Mlynek, G. Krausch, U. Steiner, *Macromolecules* **1997**, *30*, 4995.
[39] M. Boltau, S. Walheim, J. Mlynek, G. Krausch, U. Steiner, *Nature* **1998**, *391*, 877.
[40] T. Geldhauser, P. Leiderer, J. Boneberg, S. Walheim, T. Schimmel, *Langmuir* **2008**, *24*, 13155.
[41] T. Geldhauser, S. Walheim, T. Schimmel, P. Leiderer, J. Boneberg, *Macromolecules* **2010**, *43*, 1124.
[42] J. Heier, E. J. Kramer, S. Walheim, G. Krausch, *Macromolecules* **1997**, *30*, 6610.
[43] L. Rockford, Y. Liu, P. Mansky, T. P. Russell, M. Yoon, S. G. J. Mochrie, *Phys. Rev. Lett.* **1999**, *82*, 2602.
[44] Z. W. Sun, Z. B. Chen, W. X. Zhang, J. Choi, C. L. Huang, G. J. Jeong, E. B. Coughlin, Y. T. Hsu, X. M. Yang, K. Y. Lee, D. S. Kuo, S. G. Xiao, T. P. Russell, *Adv. Mater.* **2015**, *27*, 4364.
[45] S. O. Kim, H. H. Solak, M. P. Stoykovich, N. J. Ferrier, J. J. de Pablo, P. F. Nealey, *Nature* **2003**, *424*, 411.
[46] R. Sherman, D. Hirt, R. Vane, *J. Vac. Sci. Technol. A* **1994**, *12*, 1876.
[47] J. H. Maas, M. A. C. Stuart, A. B. Sieval, H. Zuilhof, E. J. R. Sudholter, *Thin Solid Films* **2003**, *426*, 135.
[48] R. Lundy, P. Yadav, A. Selkirk, E. Mullen, T. Ghoshal, C. Cummins, M. A. Morris, *Chem. Mater.* **2019**, *31*, 9338.
[49] S. Lee, T. Ishizaki, N. Saito, O. Takai, *Jpn. J. Appl. Phys.* **2008**, *47*, 6416.
[50] A. Glaser, J. Foisner, H. Hoffmann, G. Friedbacher, *Langmuir* **2004**, *20*, 5599.
[51] C. Rill, A. Glaser, J. Foisner, H. Hoffmann, G. Friedbacher, *Langmuir* **2005**, *21*, 6289.
[52] C. Huang, A. Förste, S. Walheim, T. Schimmel, *Beilstein J. Nanotechnol.* **2015**, *6*, 1205.

© 2023 The Authors. Small published by Wiley-VCH GmbH

16136829, 0, Downloaded from https://onlinelibrary.wiley.com/doi/10.1002/smll.202204962 by Karlsruher Inst F. Technologie, Wiley Online Library on [02/05/2023]. See the Terms and Conditions (https://onlinelibrary.wiley.com/terms-and-conditions) on Wiley Online Library for rules of use; OA articles are governed by the applicable Creative Commons License